Available online at www.sciencedirect.com
ScienceDirect
International Journal of Solids and Structures 44 (2007) 3811–3827
INTERNATIONAL JOURNAL OF SOLIDS and STRUCTURES
www.elsevier.com/locate/ijsolstr

On diffraction of acoustic and electric waves in piezoelectric medium by an absorbent half-plane electrode

Arman Melkumyan *

Department of Mechanics, Yerevan State University, Alex Manoogyan Str. 1, Yerevan 375025, Armenia

Received 14 April 2006; received in revised form 27 September 2006
Available online 24 October 2006

Abstract

Diffraction of incident acoustic and incident electric waves in a transversally isotropic piezoelectric medium at the boundary of a half-plane absorbent electrode is systematically investigated using the quasi-hyperbolic approximation. The electrode is assumed to be very thin so that its thickness and stiffness can be neglected. By exact inversion, the explicit expressions for the scattering waves are obtained. A closed form solution is obtained by applying Laplace transformations and the Wiener–Hopf technique. By means of the Cagniard–de Hoop method a detailed investigation of the structure of the electro-acoustic wave is conducted. The mode conversion between electric and acoustic waves, the effect of electro-acoustic head wave, the Bleustein–Gulyaev surface wave and the structure of the wave in terms of the type of the incident wave (acoustic or electric) and its angle of incidence are analyzed in detail. It is shown that in piezoelectric materials, absorbent electrodes are neither completely opaque nor completely transparent to electric and acoustic waves. The dynamic field intensity factors at the tip of the electrode are functions of the angle of incidence and time; they are derived explicitly and discussed through a detailed numerical analysis.

Keywords: Transient wave propagation; Wave scattering; Piezoelectric material; Dynamic fracture; Wiener–Hopf technique; Surface wave

1. Introduction

During recent years, piezoelectric materials have been extensively used as transducers, actuators, sensors, etc. for active vibration and acoustic control in smart materials and in the technology of structures. In piezoelectric materials, both electrical and mechanical disturbances are present which can result in a high stress evolution leading to possible fracture. At this point, the analysis of dynamic fracture problems for piezoelectric materials becomes particularly important. A number of researchers worldwide have contributed to our understanding of the dynamic problem. Investigations of piezoelectric materials containing various cracks and electrodes have been undertaken and many analytical and numerical results have been obtained. For example, the response of piezoelectric materials to impact loadings has been investigated by Parton and Kudryavtsev

* Tel. +374 91 482977.
E-mail address: melk_arman@yahoo.com

0020-7683/$ - see front matter
doi:10.1016/j.ijsolstr.2006.10.022

(1988); Li and Mataga (1996a,b); Chen and Meguid (2000); Meguid and Chen (2001); Gu et al. (2002a,b); Ueda (2003a); Li and Tang (2003); Ing and Wang (2004a,b) and incident waves' scattering in piezoelectric materials has been investigated by Narita and Shindo (1998); Shindo et al. (1999); Gu et al. (2002); Ueda (2003b); Ma et al. (2005); Grigoryan and Melkumyan (2004, 2005a,b). The results presented by Li and Mataga (1996a) and by Ing and Wang (2004a,b) contained incorrect conclusions and plots and were corrected by the present author (Melkumyan, 2005a,b).

In all these papers, authors have adopted the quasi-static approximation for piezoelectric materials. The quasi-static approximation leads to a system of hyperbolic and elliptic partial differential equations, and the detailed analysis of the transient response in piezoelectric materials using that approximation is not attainable.

The fully coupled Christoffel–Maxwell and Euler–Maxwell equations are hard to investigate, and as stated the quasi-static approximation does not allow detailed transient analysis. The situation has been improved by Li (2000), who proposed the so-called "quasi-hyperbolic approximation" for piezoelectric materials in class 6 mm, which leads to a simple system of equations with preserved hyperbolicity. Based on this approximation, Li (2001) studied the Sommerfeld problem of diffraction at the boundary of a half-plane, Li et al. (2005) investigated the scattering of waves by a crack, To et al. (2005) analyzed the scattering of waves by an interfacial crack, To et al. (2006) solved the problem on interfacial crack propagation in dissimilar piezoelectric materials. The present author studied the diffraction of nonstationary waves generated by a concentrated force (Melkumyan, 2005c), investigated dynamic semi-infinite permeable crack's propagation in piezoelectric materials (Melkumyan, 2005d) and studied the diffraction of electric and acoustic waves at the boundary of half-plane permeable crack in piezoelectric materials (Melkumyan, 2006). However, all the studies done so far consider situations where a crack is present in the media, but the diffraction at the boundary of an electrode which is embedded into an otherwise continuous piezoelectric medium has not been studied – this is analysed here.

This paper aims to present a systematic transient theoretical and numerical investigation on the diffraction of electric and acoustic waves at the boundary of a half-plane absorbent electrode. The electrode which is located at the positive part of the X axis is assumed to be absorbent and very thin, so that its thickness and stiffness can be neglected. The boundary conditions corresponding to the electrode are:

$$\varphi|_{y=0^+} = \varphi|_{y=0^-} = 0, \quad w|_{y=0^+} = w|_{y=0^-}, \quad \sigma_{yz}|_{y=0^+} = \sigma_{yz}|_{y=0^-} \quad \text{for } 0 < x < +\infty. \tag{1}$$

The Laplace integral transformations are used to bring the problem to a functional equation which is solved by applying the Wiener–Hopf technique (Noble, 1958). The solution in the time-space domain is obtained by using the Cagniard–de Hoop method (Cagniard, 1939; de Hoop, 1960). The structure of the waves and the dynamic field intensity factors at the electrode tip are derived explicitly and investigated for two wave types, that is, acoustic or electric and various angles of incidence for each. It is shown that the electro-acoustic head waves and the Bleustein–Gulyayev surface waves are disturbed by both the electric and the acoustic incident waves.

2. Problem statement

Consider a transversely isotropic piezoelectric medium of hexagonal symmetry (e.g. 6 mm class), which contains a half-plane absorbent very thin electrode. A Cartesian coordinate system XYZ is chosen in a way that the Z axis coincides with the axis of symmetry of the material, and the half-plane $0 < x < +\infty$, $y = 0$, $-\infty < z < +\infty$ coincides with the electrode.

The relevant electro-acoustic coupling is between the anti-plane displacement and the in-plane electric field, i.e

$$\mathbf{u} = (0, 0, w(x, y, t)), \quad \mathbf{E} = (-\partial\varphi(x, y, t)/\partial x, -\partial\varphi(x, y, t)/\partial y, 0), \tag{2}$$

which leads to the coupling between SH acoustic waves and TE electric waves.

Defining $\bar{c}_{44} = c_{44} + e_{15}^2\varepsilon_{11}^{-1}$, $c_\ell = s_\ell^{-1} = (\varepsilon_{11}\mu_0)^{-1/2}$, $c_\mathrm{a} = s_\mathrm{a}^{-1} = \sqrt{\bar{c}_{44}/\rho}$, $C_\mathrm{f} = c_\ell^2/(c_\ell^2 - c_\mathrm{a}^2)$ and $\tilde{c}_{44} = \bar{c}_{44}\left[1 - (1 - C_\mathrm{f})\frac{e_{15}^2}{\bar{c}_{44}\varepsilon_{11}}\right]$, where c_a and c_ℓ are the velocities of acoustic and electric waves in the piezoelectric material respectively and introducing a pseudo-electric potential function

$$\psi(x,y,t) = \varphi(x,y,t) - e_{15}C_f\varepsilon_{11}^{-1}w(x,y,t) \tag{3}$$

the following system of decoupled wave equations (Li, 2000) is obtained:

$$\frac{\partial^2 w}{\partial x^2} + \frac{\partial^2 w}{\partial y^2} - \frac{1}{c_a^2}\frac{\partial^2 w}{\partial t^2} = 0, \quad \frac{\partial^2 \psi}{\partial x^2} + \frac{\partial^2 \psi}{\partial y^2} - \frac{1}{c_\ell^2}\frac{\partial^2 \psi}{\partial t^2} = 0. \tag{4}$$

The relevant constitutive equations under the quasi-hyperbolic approximation are

$$\sigma_{xz} = \tilde{c}_{44}\frac{\partial w}{\partial x} + e_{15}\frac{\partial \psi}{\partial x}, \quad \sigma_{yz} = \tilde{c}_{44}\frac{\partial w}{\partial y} + e_{15}\frac{\partial \psi}{\partial y}, \tag{5}$$

$$D_x = e_{15}(1 - C_f)\frac{\partial w}{\partial x} - \varepsilon_{11}\frac{\partial \psi}{\partial x}, \quad D_y = e_{15}(1 - C_f)\frac{\partial w}{\partial y} - \varepsilon_{11}\frac{\partial \psi}{\partial y}. \tag{6}$$

From infinity an acoustic wave $w^{(i)}(x,y,t)$ and an electric wave $\psi^{(i)}(x,y,t)$ are incident on the electrode at arbitrary angles $\theta_a \in [0,\pi/2]$, $\theta_\ell \in [0,\pi/2]$, respectively (see Fig. 1):

$$w^{(i)}(x,y,t) = w_0 G_a(t - s_a[x\cos(\theta_a) + y\sin(\theta_a)]); \tag{7}$$

$$\psi^{(i)}(x,y,t) = \psi_0 G_\ell(t - s_\ell[x\cos(\theta_\ell) + y\sin(\theta_\ell)]), \tag{8}$$

where

$$G_a(t) = \int_0^t g_a(\tau)\,d\tau, \quad G_\ell(t) = \int_0^t g_\ell(\tau)\,d\tau; \tag{9}$$

$$g_a(\tau) = 0, \quad g_\ell(\tau) = 0, \quad \text{when } \tau < 0. \tag{10}$$

In Eqs. (7) and (8), the superscript "(i)" indicates incident waves and w_0, ψ_0 are the amplitude of the acoustic incident wave and the amplitude of the electric incident wave, respectively.

Now the incident electric potential can be determined from Eq. (3) as follows:

$$\varphi^{(i)}(x,y,t) = \psi^{(i)}(x,y,t) + e_{15}C_f\varepsilon_{11}^{-1}w^{(i)}(x,y,t). \tag{11}$$

Since the incident waves are known, the total solution $w(x,y,t)$, $\psi(x,y,t)$ can be represented in the form

$$w(x,y,t) = w^{(i)}(x,y,t) + w^{(s)}(x,y,t), \quad \psi(x,y,t) = \psi^{(i)}(x,y,t) + \psi^{(s)}(x,y,t) \tag{12}$$

where $w^{(s)}$, $\psi^{(s)}$ represent the scattering waves and are the new unknown functions to be determined (the superscript "(s)" indicates scattering wave).

Using Eqs. (5)–(8), (11)–(12) the boundary conditions (1) on the electrode can be written in the following form, where $0 < x < +\infty$:

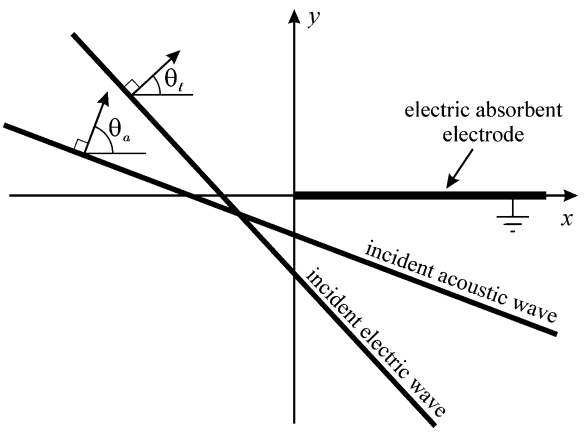

Fig. 1. Illustration of the acoustic and electric incident waves approaching the electrode.

$$\begin{aligned}
&\psi^{(s)}|_{y=0^+} + e_{15}\varepsilon_{11}^{-1}C_f w^{(s)}|_{y=0^+} = \psi^{(s)}|_{y=0^-} + e_{15}\varepsilon_{11}^{-1}C_f w^{(s)}|_{y=0^-} = -\psi^{(i)}|_{y=0} - e_{15}\varepsilon_{11}^{-1}C_f w^{(i)}|_{y=0},\\
&\tilde{c}_{44}\frac{\partial w^{(s)}}{\partial y}|_{y=0^+} + e_{15}\frac{\partial \psi^{(s)}}{\partial y}|_{y=0^+} = \tilde{c}_{44}\frac{\partial w^{(s)}}{\partial y}|_{y=0^-} + e_{15}\frac{\partial \psi^{(s)}}{\partial y}|_{y=0^-}, \quad w^{(s)}|_{y=0^+} = w^{(s)}|_{y=0^-}.
\end{aligned} \tag{13}$$

As the scattering waves are produced after the incident wave reaches the electrode, which takes place when $t = 0$, the following initial conditions apply to the scattering field:

$$w^{(s)}(x,y,0) = 0, \partial w^{(s)}(x,y,t)/\partial t|_{t=0} = 0, \quad \psi^{(s)}(x,y,0) = 0, \partial \psi^{(s)}(x,y,t)/\partial t|_{t=0} = 0 \tag{14}$$

The radiation and the edge conditions must also be satisfied.

3. Leading to a Wiener–Hopf equation and its solution

To bring the problem to a Wiener–Hopf equation, divide the piezoelectric medium into two parts: $y > 0$ and $y < 0$ satisfying the following contact conditions on the plane $y = 0$:

$$w(x,0^+,t) = w(x,0^-,t), \quad \sigma_{yz}(x,0^+,t) = \sigma_{yz}(x,0^-,t) \tag{15}$$

$$\varphi(x,0^+,t) = \varphi(x,0^-,t) = \varphi_-(x,t), \quad D_y(x,0^+,t) - D_y(x,0^-,t) = -\varepsilon_{11}D_+(x,t) \tag{16}$$

where

$$\varphi_-(x,t) = 0, \quad \text{if } x > 0; \qquad D_+(x,t) = 0, \quad \text{if } x < 0. \tag{17}$$

Applying the following one sided Laplace transform over time t

$$f^*(x,p) = \int_0^\infty f(x,t)\mathrm{e}^{-pt}\,\mathrm{d}t, \quad f(x,t) = \frac{1}{2\pi \mathrm{i}}\int_{p_0-\mathrm{i}\infty}^{p_0+\mathrm{i}\infty} f^*(x,p)\mathrm{e}^{pt}\,\mathrm{d}p \tag{18}$$

and the following two sided Laplace transform over the spatial coordinate x

$$\hat{f}^*(\zeta,p) = \int_{-\infty}^{\infty} f^*(x,p)\mathrm{e}^{-px\zeta}\,\mathrm{d}x, \quad f^*(x,p) = \frac{p}{2\pi \mathrm{i}}\int_{\zeta_0-\mathrm{i}\infty}^{\zeta_0+\mathrm{i}\infty} \hat{f}^*(\zeta,p)\mathrm{e}^{px\zeta}\,\mathrm{d}\zeta \tag{19}$$

to the wave Eqs. (4), using Eqs. (7)–(12) and the initial conditions Eq. (14) together with the radiation conditions the following system of differential equations is obtained:

$$\frac{\partial^2 \hat{w}^{(s)*}(\zeta,y,p)}{\partial y^2} - p^2a^2(\zeta)\hat{w}^{(s)*}(\zeta,y,p) = 0, \quad \frac{\partial^2 \hat{\psi}^{(s)*}(\zeta,y,p)}{\partial y^2} - p^2e^2(\zeta)\hat{\psi}^{(s)*}(\zeta,y,p) = 0, \tag{20}$$

where $a(\zeta) = \sqrt{s_a^2 - \zeta^2}$, $e(\zeta) = \sqrt{s_\ell^2 - \zeta^2}$. The single valued branch of the function $a(\zeta)$ is defined by the branch cut $\{\mathrm{Im}\,\zeta = 0, |\mathrm{Re}\,\zeta| \geqslant s_a\}$ and the condition $a(0) = s_a$. Similarly, the single valued branch of the function $e(\zeta)$ is defined by the branch cut $\{\mathrm{Im}\,\zeta = 0, |\mathrm{Re}\,\zeta| \geqslant s_\ell\}$ and the condition $e(0) = s_\ell$.

Expressing the contact conditions (15), (16) via functions $w^{(s)}$, $\psi^{(s)}$ and $w^{(i)}$, $\psi^{(i)}$ one obtains

$$\psi^{(s)}(x,0^+,t) + e_{15}C_f\varepsilon_{11}^{-1}w^{(s)}(x,0^+,t) = g_-(x,t) - \varphi_+^{(i)}(x,t); \tag{21}$$

$$\psi^{(s)}(x,0^+,t) = \psi^{(s)}(x,0^-,t); \tag{22}$$

$$w^{(s)}(x,0^+,t) = w^{(s)}(x,0^-,t); \tag{23}$$

$$\frac{\partial \psi^{(s)}}{\partial y}|_{y=0^+} - \frac{\partial \psi^{(s)}}{\partial y}|_{y=0^-} = \frac{C_f}{C_f + k_e^2(1-C_f)}D_+(x,t); \tag{24}$$

$$\frac{\partial w^{(s)}}{\partial y}|_{y=0^+} - \frac{\partial w^{(s)}}{\partial y}|_{y=0^-} = -\frac{e_{15}}{\tilde{c}_{44}}\frac{C_f}{C_f + k_e^2(1-C_f)}D_+(x,t), \tag{25}$$

where $k_e = \sqrt{C_f/(\varepsilon_{11}\tilde{c}_{44})}e_{15}$ is the electro-mechanical coupling coefficient, $U(x)$ is the unit step function,

$$g_-(x,t) = \varphi_-(x,t) - \varphi_-^{(i)}(x,t), \quad \varphi_+^{(i)}(x,t) = \varphi^{(i)}(x,0,t)U(x), \quad \varphi_-^{(i)}(x,t) = \varphi^{(i)}(x,0,t)U(-x) \tag{26}$$

and according to Eqs. (11) and (7), (8)

$$\varphi^{(\mathrm{i})}(x,0,t) = \psi_0 G_\ell(t - s_\ell x\cos\theta_\ell) + w_0 e_{15} C_\mathrm{f} \varepsilon_{11}^{-1} G_\mathrm{a}(t - s_\mathrm{a} x\cos\theta_\mathrm{a}). \tag{27}$$

The solution of Eq. (20) which satisfies Eqs. (22), (23) and the radiation condition at infinity has the form

$$\hat{w}^{(\mathrm{s})*}(\zeta,y,p) = B(\zeta,p)\mathrm{e}^{-pa(\zeta)|y|}, \quad \hat{\psi}^{(\mathrm{s})*}(\zeta,y,p) = C(\zeta,p)\mathrm{e}^{-pe(\zeta)|y|}. \tag{28}$$

Applying the integral transformations Eqs. (18) and (19) to the boundary conditions Eq. (21)–(25) and substituting into them Eq. (28) one obtains

$$B(\zeta,p) = \frac{1}{2p}\frac{e_{15}}{\tilde{c}_{44}}\frac{C_\mathrm{f}}{C_\mathrm{f} + k_\mathrm{e}^2(1-C_\mathrm{f})}\frac{\hat{D}_+^*(\zeta,p)}{a(\zeta)}, \quad C(\zeta,p) = -\frac{1}{2p}\frac{C_\mathrm{f}}{C_\mathrm{f} + k_\mathrm{e}^2(1-C_\mathrm{f})}\frac{\hat{D}_+^*(\zeta,p)}{e(\zeta)} \tag{29}$$

and the following Wiener–Hopf functional equation

$$-\frac{1}{2p}\frac{(1-k_\mathrm{e}^2)C_\mathrm{f}}{C_\mathrm{f} + k_\mathrm{e}^2(1-C_\mathrm{f})}\frac{R(\zeta)}{e(\zeta)}\hat{D}_+^*(\zeta,p) = \hat{g}_-^*(\zeta,p) - \hat{\varphi}_+^{(\mathrm{i})*}(\zeta,p), \tag{30}$$

where

$$R(\zeta) = \frac{1}{1-k_\mathrm{e}^2}\frac{a(\zeta) - k_\mathrm{e}^2 e(\zeta)}{a(\zeta)}, \tag{31}$$

$$\hat{\varphi}_+^{(\mathrm{i})*}(\zeta,p) = \frac{\psi_0 G_\ell^*(p)}{p(\zeta + s_\ell\cos\theta_\ell)} + \frac{e_{15}C_\mathrm{f}}{\varepsilon_{11}}\frac{w_0 G_\mathrm{a}^*(p)}{p(\zeta + s_\mathrm{a}\cos\theta_\mathrm{a})}. \tag{32}$$

The function $R(\zeta)$ can be factorized using Cauchy type integrals (Gakhov, 1990) by a general procedure (Achenbach, 1984; Li, 2000). The result is

$$R(\zeta) = R_+(\zeta)R_-(\zeta), \quad R_\pm(\zeta) = \frac{s_\mathrm{bge} \pm \zeta}{s_\mathrm{a} \pm \zeta}\exp\left(\frac{1}{\pi}\int_{s_\ell}^{s_\mathrm{a}} \arctan\left[k_\mathrm{e}^2\frac{\sqrt{\sigma^2 - s_\ell^2}}{\sqrt{s_\mathrm{a}^2 - \sigma^2}}\right]\frac{\mathrm{d}\sigma}{\sigma \pm \zeta}\right), \tag{33}$$

where s_bge is the Bleustein–Gulyaev wave's slowness (Bleustein, 1968; Gulyaev, 1969; Li, 2001)

$$s_\mathrm{bge} = c_\mathrm{bge}^{-1} = \sqrt{(s_\mathrm{a}^2 - k_\mathrm{e}^4 s_\ell^2)/(1-k_\mathrm{e}^4)}. \tag{34}$$

As $s_\ell < s_\mathrm{a}$, from Eq. (34) it follows that $c_\mathrm{bge} < c_\mathrm{a} < c_\ell$. Using the factorization (33) and applying the solution procedure for the Wiener–Hopf equations (Noble, 1958) to Eq. (30) one obtains that

$$\hat{D}_+^*(\zeta,p) = 2\frac{1-k_\mathrm{e}^2 c_\mathrm{a}^2 s_\ell^2}{1-k_\mathrm{e}^2}\left[\frac{\psi_0 G_\ell^*(p)}{\zeta + s_\ell\cos\theta_\ell}\frac{\sqrt{s_\ell + s_\ell\cos\theta_\ell}}{R_-(-s_\ell\cos\theta_\ell)} + \frac{e_{15}C_\mathrm{f}}{\varepsilon_{11}}\frac{w_0 G_\mathrm{a}^*(p)}{\zeta + s_\mathrm{a}\cos\theta_\mathrm{a}}\frac{\sqrt{s_\ell + s_\mathrm{a}\cos\theta_\mathrm{a}}}{R_-(-s_\mathrm{a}\cos\theta_\mathrm{a})}\right]\frac{\sqrt{s_\ell + \zeta}}{R_+(\zeta)}; \tag{35}$$

$$\begin{aligned}\hat{g}_-^*(\zeta,p) = {} & \frac{\psi_0 G_\ell^*(p)}{p(\zeta + s_\ell\cos\theta_\ell)}\left(1 - \frac{R_-(\zeta)}{\sqrt{s_\ell - \zeta}}\frac{\sqrt{s_\ell + s_\ell\cos\theta_\ell}}{R_-(-s_\ell\cos\theta_\ell)}\right) \\ & + \frac{e_{15}C_\mathrm{f}}{\varepsilon_{11}}\frac{w_0 G_\mathrm{a}^*(p)}{p(\zeta + s_\mathrm{a}\cos\theta_\mathrm{a})}\left(1 - \frac{R_-(\zeta)}{\sqrt{s_\ell - \zeta}}\frac{\sqrt{s_\ell + s_\mathrm{a}\cos\theta_\mathrm{a}}}{R_-(-s_\mathrm{a}\cos\theta_\mathrm{a})}\right).\end{aligned} \tag{36}$$

From Eqs. (28), (29) and (35) the unknown functions $\hat{w}^{(\mathrm{s})*}$, $\hat{\psi}^{(\mathrm{s})*}$ are determined and after inverting the two sided Laplace transform over the spatial coordinate x one has that

$$w^{(\mathrm{s})*}(x,y,p) = \frac{w_0 k_\mathrm{e}^2}{1-k_\mathrm{e}^2}\frac{\sqrt{s_\ell + s_\mathrm{a}\cos\theta_\mathrm{a}}}{R_-(-s_\mathrm{a}\cos\theta_\mathrm{a})}J_\mathrm{a}^{\mathrm{a}*}(x,y,p) + \frac{\psi_0}{1-k_\mathrm{e}^2}\frac{e_{15}}{\tilde{c}_{44}}\frac{\sqrt{2s_\ell}\cos(\theta_\ell/2)}{R_-(-s_\ell\cos\theta_\ell)}J_\ell^{\mathrm{a}*}(x,y,p); \tag{37}$$

$$\psi^{(\mathrm{s})*}(x,y,p) = -\frac{w_0}{1-k_\mathrm{e}^2}\frac{e_{15}C_\mathrm{f}}{\varepsilon_{11}}\frac{\sqrt{s_\ell + s_\mathrm{a}\cos\theta_\mathrm{a}}}{R_-(-s_\mathrm{a}\cos\theta_\mathrm{a})}J_\mathrm{a}^{\ell*}(x,y,p) - \frac{\psi_0}{1-k_\mathrm{e}^2}\frac{\sqrt{2s_\ell}\cos(\theta_\ell/2)}{R_-(-s_\ell\cos\theta_\ell)}J_\ell^{\ell*}(x,y,p), \tag{38}$$

where

$$J_{\mathrm{a}}^{\mathrm{a}*}(x,y,p) = G_{\mathrm{a}}^{*}(p)\frac{1}{2\pi \mathrm{i}}\int_{\zeta_0-\mathrm{i}\infty}^{\zeta_0+\mathrm{i}\infty}\frac{\sqrt{s_\ell+\zeta}\,\mathrm{e}^{-p[a(\zeta)|y|-x\zeta]}}{(\zeta+s_{\mathrm{a}}\cos\theta_{\mathrm{a}})R_+(\zeta)a(\zeta)}\,\mathrm{d}\zeta; \tag{39}$$

$$J_{\ell}^{\mathrm{a}*}(x,y,p) = G_{\ell}^{*}(p)\frac{1}{2\pi \mathrm{i}}\int_{\zeta_0-\mathrm{i}\infty}^{\zeta_0+\mathrm{i}\infty}\frac{\sqrt{s_\ell+\zeta}\,\mathrm{e}^{-p[a(\zeta)|y|-x\zeta]}}{(\zeta+s_{\ell}\cos\theta_{\ell})R_+(\zeta)a(\zeta)}\,\mathrm{d}h\zeta; \tag{40}$$

$$J_{\mathrm{a}}^{\ell*}(x,y,p) = G_{\mathrm{a}}^{*}(p)\frac{1}{2\pi \mathrm{i}}\int_{\zeta_0-\mathrm{i}\infty}^{\zeta_0+\mathrm{i}\infty}\frac{\mathrm{e}^{-p[e(\zeta)|y|-x\zeta]}}{(\zeta+s_{\mathrm{a}}\cos\theta_{\mathrm{a}})R_+(\zeta)\sqrt{s_\ell-\zeta}}\,\mathrm{d}\zeta; \tag{41}$$

$$J_{\ell}^{\ell*}(x,y,p) = G_{\ell}^{*}(p)\frac{1}{2\pi \mathrm{i}}\int_{\zeta_0-\mathrm{i}\infty}^{\zeta_0+i\infty}\frac{\mathrm{e}^{-p[e(\zeta)|y|-x\zeta]}}{(\zeta+s_{\ell}\cos\theta_{\ell})R_+(\zeta)\sqrt{s_\ell-\zeta}}\,\mathrm{d}\zeta. \tag{42}$$

In Eqs. (39)–(42), subscripts show the type of the incident wave and superscripts show the type of the produced wave. "a" stands for acoustic waves and "ℓ" stands for electric waves.

When the electro-mechanical coupling coefficient k_{e} tends to zero the solution of the problem expressed in Eqs. (37)–(42) becomes:

$$w^{(\mathrm{s})} = 0, \quad \psi^{(\mathrm{s})*} = -\psi_0\sqrt{2s_\ell}\cos(\theta_\ell/2)\frac{G_\ell^*(p)}{2\pi \mathrm{i}}\int_{\zeta_0-\mathrm{i}\infty}^{\zeta_0+\mathrm{i}\infty}\frac{\mathrm{e}^{-p[e(\zeta)|y|-x\zeta]}}{(\zeta+s_\ell\cos\theta_\ell)\sqrt{s_\ell-\zeta}}\,\mathrm{d}\zeta. \tag{43}$$

Eqs. (43) demonstrate that if there is no coupling between the electric and elastic fields, the incident acoustic wave does not interact with the electrode, the incident electric wave diffracts from the electrode and for this result no acoustic scattered wave is produced. The study of Eqs. (43) shows that the pole at $\zeta = -s_\ell\cos\theta_\ell$ cancels the incident electric wave, which means that the absorbent electrode is completely opaque for this incident wave. In the next sections, it will be shown that the situation is qualitatively different in the case of piezoelectric materials; both acoustic and electric waves interact with the electrode and for neither wave the absorbent electrode is completely opaque or completely transparent.

4. Exact inversion

In this section, Eqs. (37)–(42) will be converted back to the physical space-time domain by an exact inversion. The exact structure of the wave front will be determined by applying the Cagniard–de Hoop method (Cagniard, 1939; de Hoop, 1960) and the Cauchy residual theorem (Gakhov, 1990). Introduce an r,θ coordinate system by the rule $x = r\cos\theta$, $|y| = r\sin\theta$, where $\theta \in [0,\pi]$ and the following functions which are the parametric representations of the Cagniard–de Hoop integration contours $\Gamma_{\mathrm{a}}^{\pm}$, $\Gamma_{\mathrm{ae}}^{\pm}$, $\Gamma_{\mathrm{e}}^{\pm}$:

$$\zeta_{\mathrm{a}}^{\pm}(r,\theta,t) = r^{-1}(-t\cos\theta \pm \mathrm{i}\sqrt{t^2-s_{\mathrm{a}}^2r^2}\sin\theta), t \in [s_{\mathrm{a}}r,+\infty); \tag{44}$$

$$\zeta_{\mathrm{ae}}(r,\theta,t) = r^{-1}(-t\cos\theta + \sqrt{s_{\mathrm{a}}^2r^2-t^2}\sin\theta), t \in [t_{\mathrm{ae}},s_{\mathrm{a}}r]; \tag{45}$$

$$\zeta_{\mathrm{ae}}^{\pm}(r,\theta,t) = \zeta_{\mathrm{ae}}(r,\theta,t) \pm \mathrm{i}\varepsilon, t \in [t_{\mathrm{ae}},s_{\mathrm{a}}r]; \tag{46}$$

$$\zeta_{\mathrm{e}}^{\pm}(r,\theta,t) = r^{-1}(-t\cos\theta \pm \mathrm{i}\sqrt{t^2-s_{\ell}^2r^2}\sin\theta), t \in [s_{\ell}r,+\infty), \tag{47}$$

where

$$t_{\mathrm{ae}} = t_{\mathrm{ae}}(r,\theta) = s_\ell x + \sqrt{s_{\mathrm{a}}^2-s_\ell^2}|y|. \tag{48}$$

Direct calculations show that the following equalities take place:

$$\frac{\partial\zeta_{\mathrm{a}}^{\pm}}{\partial t} = \pm\mathrm{i}\frac{a(\zeta_{\mathrm{a}}^{\pm}(r,\theta,t))}{\sqrt{t^2-s_{\mathrm{a}}^2r^2}}, \quad \frac{\partial\zeta_{\mathrm{e}}^{\pm}}{\partial t} = \pm\mathrm{i}\frac{e(\zeta_{\mathrm{e}}^{\pm}(r,\theta,t))}{\sqrt{t^2-s_{\ell}^2r^2}}, \quad \frac{\partial\zeta_{\mathrm{ae}}}{\partial t} = \frac{\partial\zeta_{\mathrm{ae}}^{\pm}}{\partial t} = -\frac{a(\zeta_{\mathrm{ae}}(r,\theta,t))}{\sqrt{s_{\mathrm{a}}^2r^2-t^2}}. \tag{49}$$

From Eqs. (37)–(42) it follows that the solution of the problem $w^{(\mathrm{s})}(x,y,t)$, $\psi^{(\mathrm{s})}(x,y,t)$ which represents the scattering waves in the case of incidence of both acoustic and electric plane waves can be represented as the sum of the cases when only acoustic plane wave is incidence and when only electric plane wave is incident:

$w^{(s)} = w_a^{(s)} + w_\ell^{(s)}$, $\psi^{(s)} = \psi_a^{(s)} + \psi_\ell^{(s)}$. This fact makes it reasonable to study the cases of incidence of acoustic and electric plane waves separately. This methodology has been used by many researchers (Li, 2001; Li et al., 2005; To et al., 2005; Melkumyan, 2006).

4.1. the case of the incident acoustic wave (i.e. $w_0 \neq 0, \psi_0 = 0$), when $\theta_a < \arccos(s_\ell/s_a)$

In the case of the incident acoustic wave from Eqs. (37)–(42) it follows that

$$w_a^{(s)*} = \frac{w_0 k_e^2}{1-k_e^2} \frac{\sqrt{s_\ell + s_a \cos\theta_a}}{R_-(-s_a\cos\theta_a)} \frac{G_a^*(p)}{2\pi i} \int_{\zeta_0-i\infty}^{\zeta_0+i\infty} \frac{\sqrt{s_\ell+\zeta}\, e^{-p[a(\zeta)|y|-x\zeta]}}{(\zeta + s_a\cos\theta_a)R_+(\zeta)a(\zeta)}\, d\zeta; \tag{50}$$

$$\psi_a^{(s)*} = -\frac{w_0}{1-k_e^2} \frac{e_{15}C_f}{\varepsilon_{11}} \frac{\sqrt{s_\ell + s_a\cos\theta_a}}{R_-(-s_a\cos\theta_a)} \frac{G_a^*(p)}{2\pi i} \int_{\zeta_0-i\infty}^{\zeta_0+i\infty} \frac{e^{-p[e(\zeta)|y|-x\zeta]}}{(\zeta+s_a\cos\theta_a)R_+(\zeta)\sqrt{s_\ell-\zeta}}\, d\zeta, \tag{51}$$

where subscripts "a" indicate that the incident wave is an acoustic one.

The Cagniard–de Hoop integration contours together with the branch cuts, branch points and poles of the integrands of Eqs. (50), (51) are shown in Fig. 2.

Changing the integration contours in Eqs. (50), (51) from the Bromwich paths to the contour $\Gamma_a^- + \Gamma_{ae}^- + \Gamma_{ae}^+ + \Gamma_a^+$ for $w_a^{(s)*}$ and to the contour $\Gamma_e^- + \Gamma_e^+$ for $\psi_a^{(s)*}$, taking into consideration the poles and changing the variable of integration using Eqs. (44)–(49) the following expression for $w_a^{(s)}$ is obtained:

$$w_a^{(s)}(x,y,t) = -w_0 U(\theta_a-\theta)\frac{k_e^4}{1-k_e^4}\frac{s_a^2\cos^2\theta_a - s_\ell^2}{s_{bge}^2 - s_a^2\cos^2\theta_a} G_a(t - s_a[x\cos\theta_a + |y|\sin\theta_a]) + \int_0^t G_a(t-\tau) w_{a\delta}^{(s)}(x,y,\tau)\, d\tau, \tag{52}$$

where

$$w_{a\delta}^{(s)}(x,y,t) = \frac{w_0 k_e^2}{1-k_e^2}\frac{\sqrt{s_\ell + s_a\cos\theta_a}}{R_-(-s_a\cos\theta_a)} \times \left\{ \frac{1}{\pi} \mathrm{Re}\left[\frac{\sqrt{s_\ell+\zeta_a^+(t)}}{(\zeta_a^+(t)+s_a\cos\theta_a)R_+(\zeta_a^+(t))}\right] \frac{U(t-s_a r)}{\sqrt{t^2-s_a^2r^2}} - \frac{U(\arccos(s_\ell/s_a)-\theta)}{\pi} \right. \times \left. \mathrm{Re}\left[\frac{\sqrt{-\zeta_{ae}(t)-s_\ell}}{(\zeta_{ae}(t)+s_a\cos\theta_a)R_+(\zeta_{ae}(t)+i0)}\right] \frac{U(t-t_{ae})-U(t-s_a r)}{\sqrt{s_a^2r^2-t^2}} \right\}, \tag{53}$$

and the following expression for $\psi_a^{(s)}(x,y,t)$:

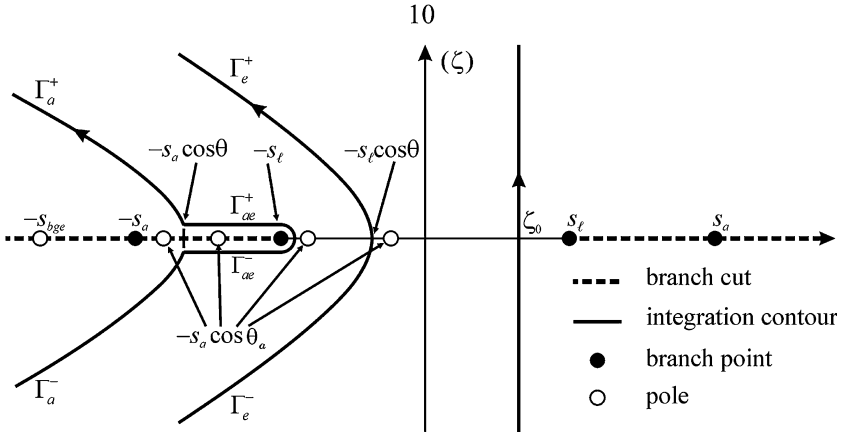

Fig. 2. Cagniard–de Hoop contours, branch cuts, branch points and poles in the case of incident acoustic wave.

$$\psi_{\mathrm{a}}^{(\mathrm{s})}(x,y,t)=\int_0^t G_{\mathrm{a}}(t-\tau)\psi_{\mathrm{a}\delta}^{(\mathrm{s})}(x,y,\tau)\,\mathrm{d}\tau, \tag{54}$$

where

$$\psi_{\mathrm{a}\delta}^{(\mathrm{s})}(x,y,t)=-\frac{w_0}{1-k_{\mathrm{e}}^2}\frac{e_{15}C_{\mathrm{f}}}{\varepsilon_{11}}\frac{\sqrt{s_\ell+s_{\mathrm{a}}\cos\theta_{\mathrm{a}}}}{R_-(-s_{\mathrm{a}}\cos\theta_{\mathrm{a}})}\frac{1}{\pi}\mathrm{Re}\left[\frac{\sqrt{s_\ell+\zeta_{\mathrm{e}}^+(t)}}{(\zeta_{\mathrm{e}}^+(r,\theta,t)+s_{\mathrm{a}}\cos\theta_{\mathrm{a}})R_+\left(\zeta_{\mathrm{e}}^+(t)\right)}\right]\frac{U(t-s_\ell r)}{\sqrt{t^2-s_\ell^2r^2}}. \tag{55}$$

The structure of the electro-acoustic waves corresponding to this case, which is obtained from the analysis of Eqs. (52)–(55) is shown in Fig. 3 where the following seven wave zones appear:

1. incident acoustic wave zone
2. acoustic wave scattering zone
3. acoustic wave reflection zone
4. acoustic wave refraction zone
5. electric wave scattering zone
6. electro-acoustic head wave zone
7. undisturbed zone

4.2. The case of the incident acoustic wave (i.e. $w_0 \neq 0$, $\psi_0 = 0$), when $\theta_a > \arccos(s_\ell/s_a)$

Undertaking the analysis using method similar to the one described in the previous case, it is found that

$$w_{\mathrm{a}}^{(\mathrm{s})}(x,y,t)=U(\theta_{\mathrm{a}}-\theta)\frac{w_0k_{\mathrm{e}}^2}{1-k_{\mathrm{e}}^2}\frac{\sqrt{s_\ell^2-s_{\mathrm{a}}^2\cos^2\theta_{\mathrm{a}}}}{R(s_{\mathrm{a}}\cos\theta_{\mathrm{a}})s_{\mathrm{a}}\sin\theta_{\mathrm{a}}}G_{\mathrm{a}}(t-s_{\mathrm{a}}[x\cos\theta_{\mathrm{a}}+|y|\sin\theta_{\mathrm{a}}])$$
$$+\int_0^t G_{\mathrm{a}}(t-\tau)w_{\mathrm{a}\delta}^{(\mathrm{s})}(x,y,\tau)\,\mathrm{d}\tau; \tag{56}$$

$$\psi_{\mathrm{a}}^{(\mathrm{s})}(x,y,t)=-\frac{U\left[\arccos\left(s_{\mathrm{a}}s_\ell^{-1}\cos\theta_{\mathrm{a}}\right)-\theta\right]}{e(s_{\mathrm{a}}\cos\theta_{\mathrm{a}})}\frac{w_0}{1-k_{\mathrm{e}}^2}\frac{e_{15}C_{\mathrm{f}}}{\varepsilon_{11}}\frac{\sqrt{s_\ell^2-s_{\mathrm{a}}^2\cos^2\theta_{\mathrm{a}}}}{R(s_{\mathrm{a}}\cos\theta_{\mathrm{a}})}$$
$$\times G_{\mathrm{a}}(t-[e(s_{\mathrm{a}}\cos\theta_{\mathrm{a}})|y|+s_{\mathrm{a}}x\cos\theta_{\mathrm{a}}])+\int_0^t G_{\mathrm{a}}(t-\tau)\psi_{\mathrm{a}\delta}^{(\mathrm{s})}(x,y,\tau)\,\mathrm{d}\tau, \tag{57}$$

where $w_{\mathrm{a}\delta}^{(\mathrm{s})}(x,y,t)$ is defined in Eq. (53) and $\psi_{\mathrm{a}\delta}^{(\mathrm{s})}(x,y,t)$ is defined in Eq. (55).

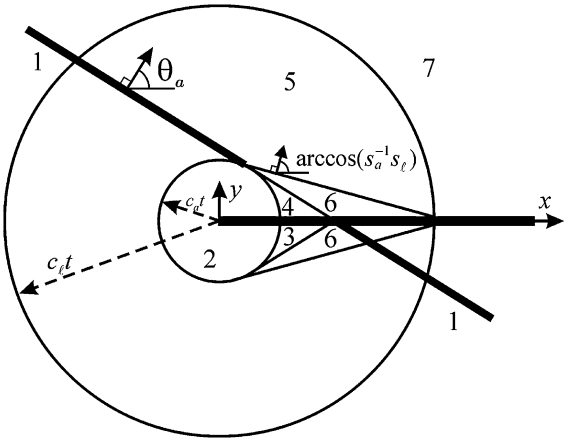

Fig. 3. The structure of the waves in the case of the incident acoustic wave when $\theta_{\mathrm{a}} < \arccos(s_\ell/s_{\mathrm{s}})$.

The structure of the electro-acoustic waves corresponding to this case [Eqs. (56), (57), (53) and (55)] is shown in Fig. 4, where the following nine wave zones appear:

1. incident acoustic wave zone
2. acoustic wave scattering zone
3. acoustic wave reflection zone
4. acoustic wave refraction zone
5. electric wave scattering zone
6. electro-acoustic head wave zone
7. electric wave reflection zone
8. electric wave refraction zone
9. undisturbed zone

4.3. The case of the incident electric wave (i.e. $w_0 = 0$, $\psi_0 \neq 0$) for any θ_ℓ

In the case of the incident electric wave from Eqs. (37) and (38), it follows that

$$w_\ell^{(s)*}(x,y,p) = \frac{\psi_0}{1-k_e^2}\frac{e_{15}}{\tilde{c}_{44}}\frac{\sqrt{2s_\ell}\cos(\theta_\ell/2)}{R_-(-s_\ell\cos\theta_\ell)}\frac{G_\ell^*(p)}{2\pi i}\int_{\zeta_0-i\infty}^{\zeta_0+i\infty}\frac{\sqrt{s_\ell+\zeta}\,e^{-p[a(\zeta)|y|-x\zeta]}}{(\zeta+s_\ell\cos\theta_\ell)R_+(\zeta)a(\zeta)}\,d\zeta; \tag{58}$$

$$\psi_\ell^{(s)*}(x,y,p) = -\frac{\psi_0}{1-k_e^2}\frac{\sqrt{2s_\ell}\cos(\theta_\ell/2)}{R_-(-s_\ell\cos\theta_\ell)}\frac{G_\ell^*(p)}{2\pi i}\int_{\zeta_0-i\infty}^{\zeta_0+i\infty}\frac{e^{-p[e(\zeta)|y|-x\zeta]}}{(\zeta+s_\ell\cos\theta_\ell)R_+(\zeta)\sqrt{s_\ell-\zeta}}\,d\zeta, \tag{59}$$

where subscripts "ℓ" indicate that the incident wave is an electric one.

Further analysis similar to the one conducted in the previous two cases leads to the following expression for the displacement $w_\ell^{(s)}(x,y,t)$:

$$w_\ell^{(s)}(x,y,t) = \frac{\psi_0}{1-k_e^2}\frac{e_{15}}{\tilde{c}_{44}}\frac{s_\ell\sin(\theta_\ell)}{R(s_\ell\cos\theta_\ell)}\frac{U\left[\arccos(s_a^{-1}s_\ell\cos\theta_\ell)-\theta\right]}{a(s_\ell\cos\theta_\ell)} \times G_\ell(t-[a(s_\ell\cos\theta_\ell)|y|+s_\ell x\cos\theta_\ell]) + \int_0^t G_\ell(t-\tau)w_{\ell\delta}^{(s)}(x,y,\tau)\,d\tau, \tag{60}$$

where

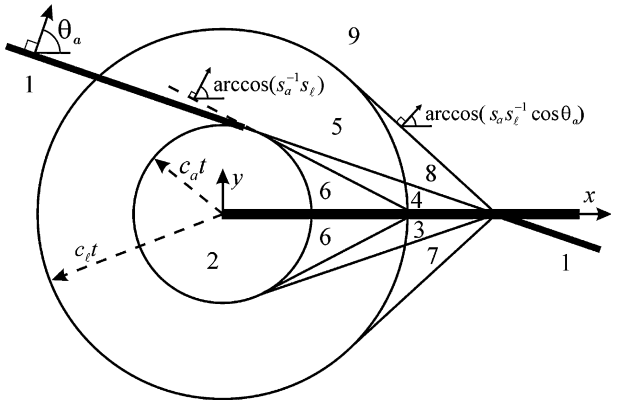

Fig. 4. The structure of the waves in the case of incident acoustic wave when $\theta_a > \arccos(s_\ell/s_s)$.

$$w_{\ell\delta}^{(s)}(x,y,t)=\frac{\psi_0}{1-k_e^2}\frac{e_{15}}{\tilde{c}_{44}}\frac{\sqrt{2s_\ell}\cos(\theta_\ell/2)}{R_-(-s_\ell\cos\theta_\ell)}\left\{\frac{1}{\pi}\mathrm{Re}\left[\frac{\sqrt{s_\ell+\zeta_a^+(t)}}{(\zeta_a^+(t)+s_\ell\cos\theta_\ell)R_+(\zeta_a^+(t))}\right]\frac{U(t-s_a r)}{\sqrt{t^2-s_a^2r^2}}\right.$$
$$\left.-\frac{U(\arccos(s_\ell/s_a)-\theta)}{\pi}\mathrm{Re}\left[\frac{\sqrt{-s_\ell-\zeta_{ae}(t)}}{(\zeta_{ae}(t)+s_\ell\cos\theta_\ell)R_+(\zeta_{ae}(t)+i0)}\right]\frac{U(t-t_{ae})-U(t-s_a r)}{\sqrt{s_a^2r^2-t^2}}\right\},\quad(61)$$

and to the following expression for the potential $\psi_\ell^{(s)}(x,y,t)$:

$$\psi_\ell^{(s)}(x,y,t)=-\frac{\psi_0}{1-k_e^2}\frac{U(\theta_\ell-\theta)}{R(-s_\ell\cos\theta_\ell)}G_\ell(t-s_\ell[x\cos\theta_\ell+|y|\sin\theta_\ell])+\int_0^t G_\ell(t-\tau)\psi_{\ell\delta}^{(s)}(x,y,\tau)\,\mathrm{d}\tau,\quad(62)$$

where

$$\psi_{\ell\delta}^{(s)}(x,y,t)=-\frac{\psi_0}{1-k_e^2}\frac{\sqrt{2s_\ell}\cos(\theta_\ell/2)}{R_-(-s_\ell\cos\theta_\ell)}\frac{1}{\pi}\mathrm{Re}\left[\frac{\sqrt{s_\ell+\zeta_e^+(t)}}{(\zeta_e^+(t)+s_\ell\cos\theta_\ell)R_+(\zeta_e^+(t))}\right]\frac{U(t-s_\ell r)}{\sqrt{t^2-s_\ell^2r^2}}.\quad(63)$$

The structure of the electro-acoustic waves corresponding to this case [Eqs. (60)–(63)] is shown in Fig. 5 where the following nine wave zones appear:

1. incident electric wave zone
2. acoustic wave scattering zone
3. acoustic wave reflection zone
4. acoustic wave refraction zone
5. electric wave scattering zone
6. electro-acoustic head wave zone
7. electric wave reflection zone
8. electric wave refraction zone
9. undisturbed zone

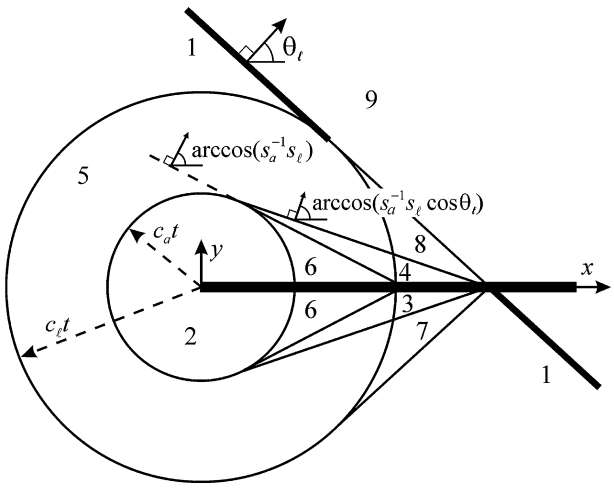

Fig. 5. The structure of the waves in the case of incident electric wave.

5. Discussion

5.1. Mode conversion and reflection coefficients

It can be seen from Eqs. (52)–(57) and (60)–(63) which represent the electro-acoustic waves in piezoelectric material that both the incident acoustic and the incident electric waves can produce scattering, as well as reflected and refracted waves of both types. To examine the mode conversion in this problem, the following reflection coefficients in the case of the incident acoustic wave are introduced:

$$R_{\mathrm{a}}^{\mathrm{a}} = \text{Amplitude of the reflected acoustic wave/Amplitude of the incident acoustic wave,} \tag{64}$$

$$R_{\mathrm{a}}^{\ell} = \text{Amplitude of the reflected electric wave/Amplitude of the incident acoustic wave,} \tag{65}$$

and the following reflection coefficients in the case of the incident electric wave

$$R_{\ell}^{\mathrm{a}} = \text{Amplitude of the reflected acoustic wave/Amplitude of the incident electric wave,} \tag{66}$$

$$R_{\ell}^{\ell} = \text{Amplitude of the reflected electric wave/Amplitude of the incident electric wave.} \tag{67}$$

From Eqs. (52)–(57) and (60)–(63) it follows that if $\theta_{\mathrm{a}} < \arccos(s_\ell/s_{\mathrm{a}})$, then

$$R_{\mathrm{a}}^{\mathrm{a}} = -\frac{k_{\mathrm{e}}^4}{1-k_{\mathrm{e}}^4}\frac{s_{\mathrm{a}}^2\cos^2\theta_{\mathrm{a}} - s_\ell^2}{s_{\mathrm{bge}}^2 - s_{\mathrm{a}}^2\cos^2\theta_{\mathrm{a}}}, \quad R_{\mathrm{a}}^{\ell} = 0; \tag{68}$$

if $\theta_{\mathrm{a}} > \arccos(s_\ell/s_{\mathrm{a}})$, then

$$R_{\mathrm{a}}^{\mathrm{a}} = \frac{k_{\mathrm{e}}^2}{1-k_{\mathrm{e}}^2}\frac{\sqrt{s_\ell^2 - s_{\mathrm{a}}^2\cos^2\theta_{\mathrm{a}}}}{R(s_{\mathrm{a}}\cos\theta_{\mathrm{a}})s_{\mathrm{a}}\sin\theta_{\mathrm{a}}}, \quad R_{\mathrm{a}}^{\ell} = -\frac{1}{e(s_{\mathrm{a}}\cos\theta_{\mathrm{a}})}\frac{1}{1-k_{\mathrm{e}}^2}\frac{e_{15}C_{\mathrm{f}}}{\varepsilon_{11}}\frac{\sqrt{s_\ell^2 - s_{\mathrm{a}}^2\cos^2\theta_{\mathrm{a}}}}{R(s_{\mathrm{a}}\cos\theta_{\mathrm{a}})}; \tag{69}$$

for any θ_ℓ

$$R_{\ell}^{\mathrm{a}} = \frac{1}{1-k_{\mathrm{e}}^2}\frac{e_{15}}{\tilde{c}_{44}}\frac{s_\ell\sin(\theta_\ell)}{R(s_\ell\cos\theta_\ell)}\frac{1}{a(s_\ell\cos\theta_\ell)}, \quad R_{\ell}^{\ell} = -\frac{1}{1-k_{\mathrm{e}}^2}\frac{1}{R(-s_\ell\cos\theta_\ell)}. \tag{70}$$

From Eqs. (64)–(70), it follows that the incident electric wave always produces reflected waves of both types, and the incident acoustic wave does not produce any reflected electric wave if $\theta_{\mathrm{a}} < \arccos(s_\ell/s_{\mathrm{a}})$. Eqs. (64)–(70) prove that the absorbent electrode is neither completely transparent nor completely opaque for acoustic and electric waves, because each of these waves is partially reflected and partially transmitted to the other side of the electrode. If $e_{15} \to 0$, then from Eqs. (68)–(70) it follows that $R_{\mathrm{a}}^{\mathrm{a}} \to 0$, $R_{\mathrm{a}}^{\ell} \to 0$, $R_{\ell}^{a} \to 0$, $R_{\ell}^{\ell} \to -1$ so that the incident acoustic wave is not reflected at all, while the incident electric wave is fully reflected. Thus, if no coupling is present between the electric and acoustic fields the absorbent electrode is completely transparent for the acoustic waves and is completely opaque for the electric waves.

5.2. Dynamic field intensity factors

Analyzing Eqs. (50), (51), (58), (59) and using Eqs. (5) and (6) one obtains that on the half-plane $y = 0$, $x < 0$ the components $\sigma_{yz}^{(\mathrm{s})}$, $\varepsilon_{yz}^{(\mathrm{s})}$, $E_y^{(\mathrm{s})}$, $D_y^{(\mathrm{s})}$ vanish, meanwhile for the case of the incident acoustic wave

$$\lim_{x\to+0}\sqrt{2\pi x}\sigma_{yz}^{(\mathrm{a})}(x,\pm0,t) = 0; \tag{71}$$

$$\lim_{x\to+0}\sqrt{2\pi x}\varepsilon_{yz}^{(\mathrm{a})}(x,\pm0,t) = \mp\frac{w_0k_{\mathrm{e}}^2}{1-k_{\mathrm{e}}^2}\frac{\sqrt{s_\ell + s_{\mathrm{a}}\cos\theta_{\mathrm{a}}}}{R_-(-s_{\mathrm{a}}\cos\theta_{\mathrm{a}})}\chi_{\mathrm{a}}(t); \tag{72}$$

$$\lim_{x\to+0}\sqrt{2\pi x}D_y^{(\mathrm{a})}(x,\pm0,t) = \mp w_0e_{15}\frac{(1-C_{\mathrm{f}})k_{\mathrm{e}}^2 + C_{\mathrm{f}}}{1-k_{\mathrm{e}}^2}\frac{\sqrt{s_\ell + s_{\mathrm{a}}\cos\theta_{\mathrm{a}}}}{R_-(-s_{\mathrm{a}}\cos\theta_{\mathrm{a}})}\chi_{\mathrm{a}}(t); \tag{73}$$

$$\lim_{x\to+0}\sqrt{2\pi x}E_y^{(\mathrm{a})}(x,\pm0,t) = \mp w_0\frac{e_{15}C_{\mathrm{f}}}{\varepsilon_{11}}\frac{\sqrt{s_\ell + s_{\mathrm{a}}\cos\theta_{\mathrm{a}}}}{R_-(-s_{\mathrm{a}}\cos\theta_{\mathrm{a}})}\chi_{\mathrm{a}}(t), \tag{74}$$

and for the case of the incident electric wave

$$\lim_{x\to+0}\sqrt{2\pi x}\sigma_{yz}^{(\ell)}(x,\pm0,t)=0; \tag{75}$$

$$\lim_{x\to+0}\sqrt{2\pi x}\varepsilon_{yz}^{(\ell)}(x,\pm0,t)=\mp\frac{\psi_0}{1-k_e^2}\frac{e_{15}}{\tilde{c}_{44}}\frac{\sqrt{2s_\ell}\cos(\theta_\ell/2)}{R_-(-s_\ell\cos\theta_\ell)}\chi_\ell(t); \tag{76}$$

$$\lim_{x\to+0}\sqrt{2\pi x}D_y^{(\ell)}(x,\pm0,t)=\mp\frac{\psi_0\varepsilon_{11}}{1-k_e^2}\frac{(1-C_f)k_e^2+C_f}{C_f}\frac{\sqrt{2s_\ell}\cos(\theta_\ell/2)}{R_-(-s_\ell\cos\theta_\ell)}\chi_\ell(t); \tag{77}$$

$$\lim_{x\to+0}\sqrt{2\pi x}E_y^{(\ell)}(x,\pm0,t)=\pm\psi_0\frac{\sqrt{2s_\ell}\cos(\theta_\ell/2)}{R_-(-s_\ell\cos\theta_\ell)}\chi_\ell(t), \tag{78}$$

where

$$\chi_a(t)=\sqrt{2/\pi}\int_0^t g_a(\tau)(t-\tau)^{-1/2}\,d\tau,\quad \chi_\ell(t)=\sqrt{2/\pi}\int_0^t g_\ell(\tau)(t-\tau)^{-1/2}\,d\tau. \tag{79}$$

From Eqs. (71)–(78), it follows that in the case of the incident acoustic wave

$$K_\varepsilon^{(a)}(\theta_a,t)=(w_0\sqrt{s_a})F_\varepsilon^{(a)}(\theta_a)\chi_a(t); \tag{80}$$

$$K_D^{(a)}(\theta_a,t)=(w_0e_{15}\sqrt{s_a})F_D^{(a)}(\theta_a)\chi_a(t);\quad K_E^{(a)}(\theta_a,t)=\left(w_0\frac{e_{15}}{\varepsilon_{11}}\sqrt{s_a}\right)F_E^{(a)}(\theta_a)\chi_a(t), \tag{81}$$

and in the case of the incident electric wave

$$K_\varepsilon^{(\ell)}(\theta_\ell,t)=\left(\psi_0\frac{e_{15}}{\tilde{c}_{44}}\sqrt{s_\ell}\right)F_\varepsilon^{(\ell)}(\theta_\ell)\chi_\ell(t); \tag{82}$$

$$K_D^{(\ell)}(\theta_\ell,t)=(\psi_0\varepsilon_{11}\sqrt{s_\ell})F_D^{(\ell)}(\theta_\ell)\chi_\ell(t);\quad K_E^{(\ell)}(\theta_\ell,t)=(\psi_0\sqrt{s_\ell})F_E^{(\ell)}(\theta_\ell)\chi_\ell(t), \tag{83}$$

where

$$F_\varepsilon^{(a)}\left(\theta_a,k_e,\frac{s_\ell}{s_a}\right)=\frac{k_e^2}{1-k_e^2}\frac{\sqrt{s_\ell s_a^{-1}+\cos\theta_a}}{R_-(-s_a\cos\theta_a)}; \tag{84}$$

$$F_D^{(a)}\left(\theta_a,k_e,\frac{s_\ell}{s_a}\right)=\frac{(1-C_f)k_e^2+C_f}{1-k_e^2}\frac{\sqrt{s_\ell s_a^{-1}+\cos\theta_a}}{R_-(-s_a\cos\theta_a)};\quad F_E^{(a)}\left(\theta_a,k_e,\frac{s_\ell}{s_a}\right)=C_f\frac{\sqrt{s_\ell s_a^{-1}+\cos\theta_a}}{R_-(-s_a\cos\theta_a)}; \tag{85}$$

$$F_\varepsilon^{(\ell)}\left(\theta_\ell,k_e,\frac{s_\ell}{s_a}\right)=\frac{1}{1-k_e^2}\frac{\sqrt{2}\cos(\theta_\ell/2)}{R_-(-s_\ell\cos\theta_\ell)}; \tag{86}$$

$$F_D^{(\ell)}\left(\theta_\ell,k_e,\frac{s_\ell}{s_a}\right)=\frac{(1-C_f)k_e^2+C_f}{(1-k_e^2)C_f}\frac{\sqrt{2}\cos(\theta_\ell/2)}{R_-(-s_\ell\cos\theta_\ell)};\quad F_E^{(\ell)}\left(\theta_\ell,k_e,\frac{s_\ell}{s_a}\right)=\frac{\sqrt{2}\cos(\theta_\ell/2)}{R_-(-s_\ell\cos\theta_\ell)}. \tag{87}$$

From Eqs. (71) and (75), it follows that stresses have no singularity at the tip of the absorbent electrode regardless of the type of the incident wave (electric or acoustic). This behavior of the absorbent electrode is unique and qualitatively different from the behaviors of both permeable cracks and conductive cracks (Melkumyan, 2006; Li et al., 2005).

Eqs. (79)–(87) show that all the intensity factors have the same structure: they can be expressed as a product of two functions the first one of which depends on the coefficients of the piezoelectric material and the angle of incidence, while the second one depends on the time and the function representing the incident wave.

From Eqs. (80)–(83) it also follows that

$$\frac{K_\varepsilon^{(a)}(\theta_a,t)}{K_\varepsilon^{(\ell)}(\theta_\ell,t)}=\frac{K_D^{(a)}(\theta_a,t)}{K_D^{(\ell)}(\theta_\ell,t)}=\frac{K_E^{(a)}(\theta_a,t)}{K_E^{(\ell)}(\theta_\ell,t)}=\frac{w_0}{\psi_0}\frac{e_{15}}{\varepsilon_{11}}\frac{\chi_a(t)}{\chi_\ell(t)}\lambda(\theta_a,\theta_\ell,k_e,s_a/s_\ell), \tag{88}$$

where

$$\lambda(\theta_a, \theta_\ell, k_e, s_\ell/s_a) = C_f \frac{\sqrt{1 + s_a s_\ell^{-1} \cos\theta_a}}{\sqrt{2}\cos(\theta_\ell/2)} \frac{R_-(-s_\ell \cos\theta_\ell)}{R_-(-s_a \cos\theta_a)}. \tag{89}$$

The relationships in Eq. (88) show that the dynamic field intensity factors corresponding to the cases of the incident acoustic wave and the incident electric wave are proportional. This fact can be important in further applications, since it enables prediction of the intensity factors for the case of the incident electric wave, if they are known for the case of the incident acoustic wave and vice versa.

Figs. 6–12 show the variations of the phase functions which describe the behavior of the corresponding intensity factors, and the variation of the universal function λ versus angles of incidence and versus the electro-mechanical coupling coefficient. The correspondence between the line styles and the values of k_e are shown in Fig. 6a and it is the same in all the (a) parts of Figs. 6 – 12. The correspondence between the line styles and the values of the angle of incidence are shown in Fig. 6b and it is the same in all the (b) parts of Figs. 6–12.

From Figs. 6–8a, it follows that in the case of the incident acoustic wave the intensity factors have different values when $\theta_a = 0°$, however all of them monotonically tend to zero when $\theta_a \to 90°$. Figs. 9–11a demonstrate that contrary to the case of the incident acoustic wave, in the case of the incident electric wave the intensity

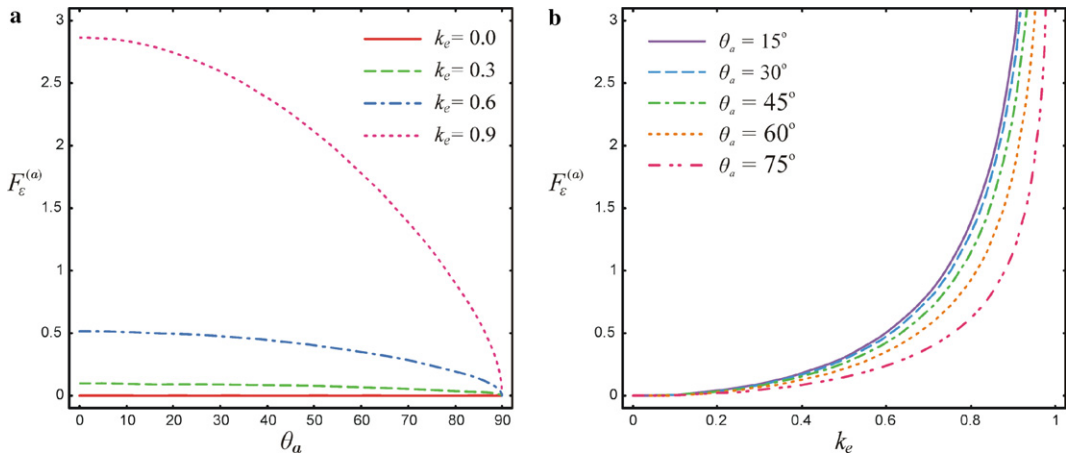

Fig. 6. The function $F_\varepsilon^{(a)}$ (a) versus θ_a for various values of k_e, (b) versus k_e for various angles of incidence θ_a.

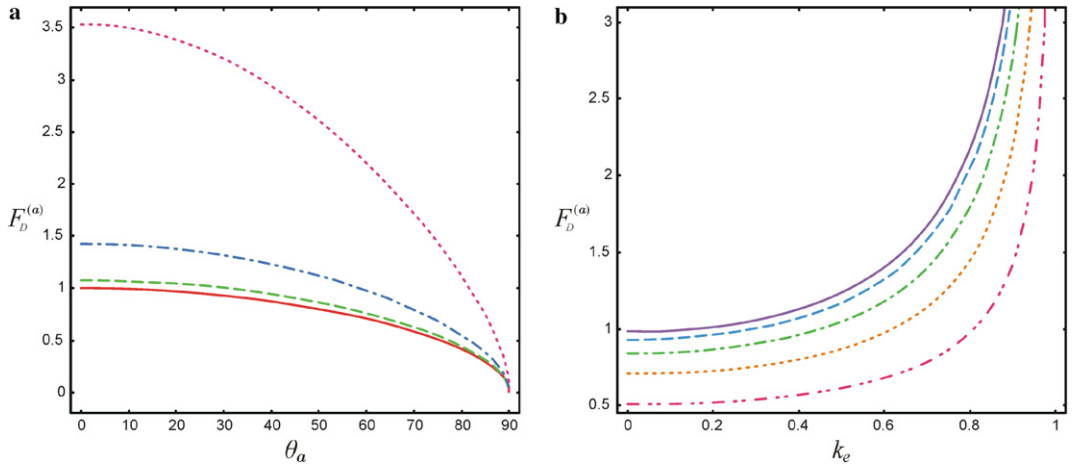

Fig. 7. The function $F_D^{(a)}$ (a) versus θ_a for various values of k_e, (b) versus k_e for various angles of incidence θ_a.

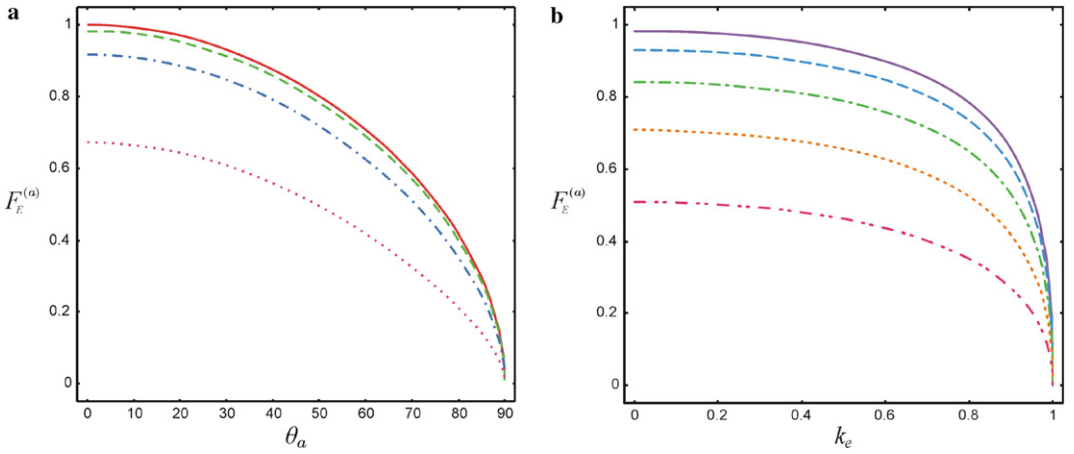

Fig. 8. The function $F_{\mathrm{E}}^{(\mathrm{a})}$ (a) versus θ_{a} for various values of k_{e}, (b) versus k_{e} for various angles of incidence θ_{a}.

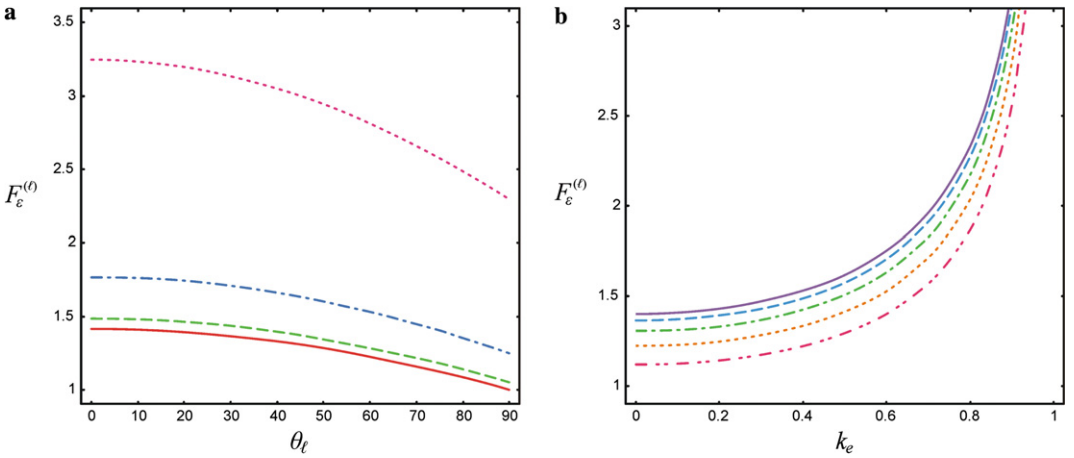

Fig. 9. The function $F_{\varepsilon}^{(\ell)}$ (a) versus θ_{ℓ} for various values of k_{e}, (b) versus k_{e} for various angles of incidence θ_{ℓ}.

factors vary monotonically from one nonzero value to another nonzero value when the angle of incidence θ_{ℓ} increases from zero to 90°.

From the dependences of the phase functions $F_{\varepsilon}^{(\mathrm{a})}$, $F_{\mathrm{D}}^{(\mathrm{a})}$ and $F_{\mathrm{E}}^{(\mathrm{a})}$ on the electro-mechanical coupling coefficient k_{e} shown in Figs. 6–8b it follows that all of them depend on k_{e} monotonically. The functions $F_{\varepsilon}^{(\mathrm{a})}$ and $F_{\mathrm{D}}^{(\mathrm{a})}$ monotonically tend to infinity when k_{e} tends to one, contrary to $F_{\mathrm{E}}^{(\mathrm{a})}$ which tends to zero when $k_{\mathrm{e}} \to 1$. Based on the fact that $F_{\varepsilon}^{(\mathrm{a})}$ vanishes and $F_{\mathrm{D}}^{(\mathrm{a})}$, $F_{\mathrm{E}}^{(\mathrm{a})}$ have finite limits when k_{e} tends to zero, from Eqs. (80) and (81) it follows that in the case of incident acoustic wave all the intensity factors vanish when the electro-mechanical coupling coefficient tends to zero. Figs. 9–11b show that $F_{\varepsilon}^{(\ell)}$ and $F_{\mathrm{D}}^{(\ell)}$ tend to infinity when the electro-mechanical coupling coefficient tends to one, contrary to $F_{\mathrm{E}}^{(\ell)}$ which tends to zero when $k_{\mathrm{e}} \to 1$. From Eqs. (82), (83) and Figs. 9–11b it follows that $K_{\sigma}^{(\ell)}$ and $K_{\varepsilon}^{(\ell)}$ vanish, while $K_{\mathrm{D}}^{(\ell)}$ and $K_{\mathrm{E}}^{(\ell)}$ have nonzero limits in the case of incident electric wave when $k_{\mathrm{e}} \to 0$.

Fig. 12 shows the dependence of the universal function λ [defined in Eqs. (88) and (89)] on the angle of incidence when $\theta_{\mathrm{a}} = \theta_{\ell}$ and on the electro-mechanical coupling coefficient. From Fig. 12a it follows that λ monotonically decreases when the incidence angle increases and tends to zero when the front of the incident wave becomes parallel to the electrode. As well as this, Fig. 12b shows that λ monotonically increases when k_{e} increases and has nonzero finite limits when $k_{\mathrm{e}} \to 0$ and $k_{\mathrm{e}} \to 1$.

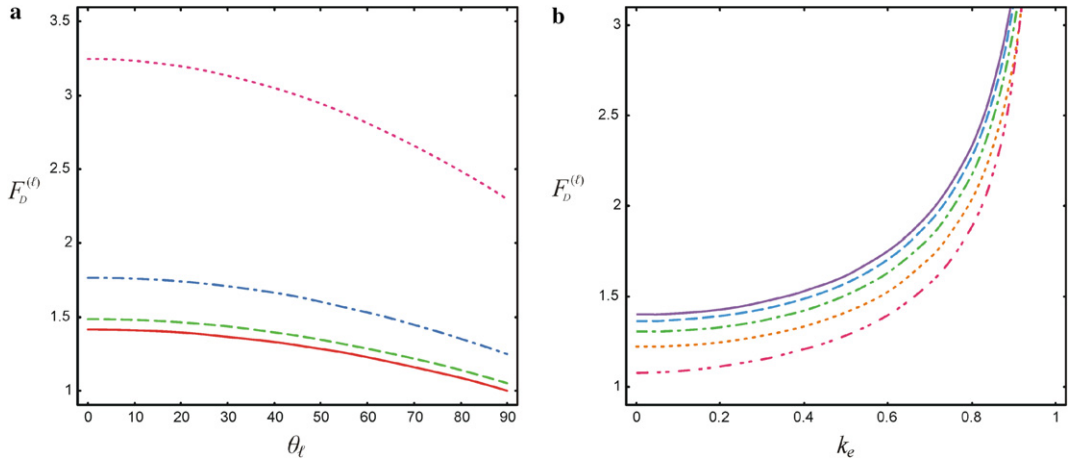

Fig. 10. The function $F_{\mathrm{D}}^{(\ell)}$ (a) versus θ_ℓ for various values of k_{e}, (b) versus k_{e} for various angles of incidence θ_ℓ.

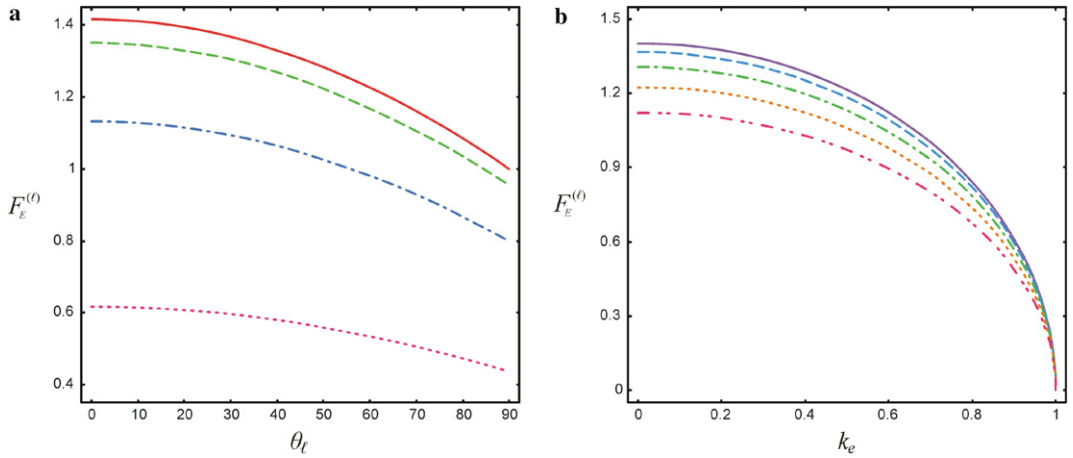

Fig. 11. The function $F_{\mathrm{E}}^{(l)}$ (a) versus θ_ℓ for various values of k_{e}, (b) versus k_{e} for various angles of incidence θ_ℓ.

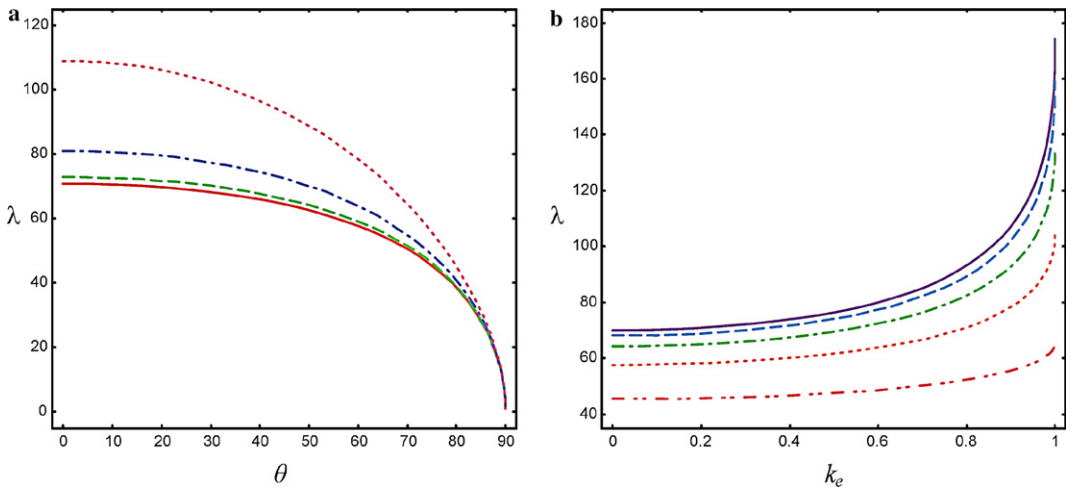

Fig. 12. The function λ (a) versus θ for various values of k_{e} and (b) versus k_{e} for various angles of incidence θ.

6. Conclusion

Diffraction of incident acoustic and incident electric waves in a transversally isotropic piezoelectric medium at the boundary of a half-plane absorbent electrode is systematically investigated using the quasi-hyperbolic approximation. The electrode is assumed to be very thin so that its thickness and stiffness can be neglected. By exact inversion, the explicit expressions for the scattering waves are obtained. A detailed analysis of the structure of the waves has shown that the incident acoustic wave can produce electric scattering waves, reflected and refracted electric waves and electro-acoustic head waves and vice-versa: the incident electric wave can produce acoustic scattering waves, acoustic reflected and refracted waves and electro-acoustic head waves due to the electro-acoustical coupling present in the piezoelectric materials. It is shown that the incident acoustic waves produce reflected and refracted electric waves if and only if the angle of incidence is greater than $\arccos(s_\ell/s_s)$, while the incident electric waves produce reflected and refracted acoustic waves for any angle of incidence. The reflection coefficients of the acoustic and the electric waves are derived explicitly. The solution has shown that the absorbent electrode is neither completely transparent nor completely opaque for both the electric and acoustic waves when the electro-mechanical coupling coefficient is not equal to zero.

Exact analytical transient expressions for the dynamic field intensity factors are obtained and expressed in explicit forms for both cases of incident acoustic and incident electric waves. It is proved that the dynamic stress intensity factor is equal to zero regardless of the type of the incident wave (electric or acoustic) and its angle of incidence. This is contrary to the case of diffraction by a permeable or conductive crack for which both the stress intensity factor and the electric displacement intensity factor are not equal to zero (Melkumyan, 2006; Li et al., 2005). It is shown that all the intensity factors have the same structure: they can be expressed as a product of two functions the first one of which depends on the coefficients of the piezoelectric material and the angle of incidence, while the second one depends on the time and the function representing the incident wave. When the electro-mechanical coupling coefficient vanishes the incident acoustic wave does not interact with the electrode, so that all the intensity factors become equal to zero. The diffraction of the incident electric wave at the boundary of the absorbent electrode takes place regardless of the electro-mechanical coupling coefficient; however when the electro-mechanical coupling coefficient vanishes, the diffraction of the electric wave does not lead to nonzero intensity factors in the elastic field.

It is shown that the angles of incidence of the acoustic and electric waves have great impact on the intensity factors in both acoustic and electric fields. All the intensity factors are monotonically dependent on the corresponding angles of incidence. In the case of the incident acoustic wave all the intensity factors vanish when the angle of incidence tends to 90° and have a nonzero limit when it tends to zero. Meanwhile, in the case of the incident electric wave all the intensity factors, except the stress intensity factor (identically equal to zero), have nonzero limits when the angle of incidence tends to zero or to 90°.

It is proved that the intensity factors generated by the incident acoustic wave are proportional to the corresponding intensity factors generated by the incident electric wave. The universal function of their ratios λ is determined in the exact explicit form and further analyzed. From this analysis it is shown that λ monotonically decreases when the angle of incidence increases and tends to zero when the incident wave's front becomes parallel to the electrode; λ monotonically increases when k_e increases, and λ has nonzero finite limits when $k_e \to 0$ and $k_e \to 1$. A detailed numerical analysis is presented for all intensity factors and for λ which describes the influences of the angle of incidence and of the electromechanical coupling coefficient.

References

Achenbach, J.D., 1984. Wave Propagation in Elastic Solids. North-Holland, Amsterdam.

Bleustein, J.L., 1968. A new surface wave in piezoelectric materials. Appl. Phys. Letters 13, 412–413.

Cagniard, L., 1939. Reflection and Refraction of Progressive Seismic Waves. Gauthier-Villars, Paris.

Chen, Z.T., Meguid, S.A., 2000. The transient response of a piezoelectric strip with a vertical crack under electromechanical impact load. Int. J. Solids Struct. 37, 6051–6062.

de Hoop, A.T., 1960. A modification of Cagniard's method for solving seismic pulse problems. Appl. Sci. Res. B8, 349–360.

Gakhov, F.D., 1990. Boundary Value Problems. Dover Publications, New York.

Grigoryan, E., Melkumyan, A., 2004. On wave diffraction in a piezoelectric medium containing a semi-infinite electrode. In Proceedings of the International Seminar "Day on Diffraction' 2004", St. Petersburg, pp. 100–109.

Grigoryan, E., Melkumyan, A., 2005a. Diffraction of shear plane waves in piezoelectric media on the edges of parallel semi-infinite metallic strips. Proc. Natl. Acad. Sci. Armenia, Mech. 58 (3), 16–28.

Grigoryan, E., Melkumyan, A., 2005b. On diffraction in a piezoelectric medium by parallel-situated electrodes. In: Proceedings of The 4th Australasian Congress on Applied Mechanics (ACAM 2005). The National Committee on Applied Mechanics, Melbourne, pp. 93–598.

Gu, B., Yu, S.-W., Feng, X.-Q., 2002a. Transient response of an interface crack between dissimilar piezoelectric layers under mechanical impacts. Int. J. Solids Struct. 39, 1743–1756.

Gu, B., Yu, S.-W., Feng, X.-Q., 2002b. Transient response of an insulating crack between dissimilar piezoelectric layers under mechanical and electrical impacts. Arch. Appl. Mech. 72, 615–629.

Gu, B., Yu, S.-W., Feng, X.-Q., Mai, Y.-W., 2002. Scattering of love waves by an interface crack between a piezoelectric layer and an elastic substrate. Acta Mechanica Solida Sinica 15, 111–118.

Gulyaev, Y.V., 1969. Electroacoustic surface waves in solids. Soviet Phys. JETP 9, 37–38.

Ing, Y.S., Wang, M.J., 2004a. Explicit transient solutions for a mode III crack subjected to dynamic concentrated loading in a piezoelectric material. Int. J. Solids Struct. 41, 3849–3864.

Ing, Y.S., Wang, M.J., 2004b. Transient analysis for a mode-III crack propagating in a piezoelectric material. Int. J. Solids Struct. 41, 6197–6214.

Li, S., Mataga, P.A., 1996a. Dynamic crack propagation in piezoelectric materials Part I: electrode solution. J. Mech. Phys. Solids 44, 1799–1830.

Li, S., Mataga, P.A., 1996b. Dynamic crack propagation in piezoelectric materials Part II: vacuum solution. J. Mech. Phys. Solids 44, 1831–1866.

Li, S., 2000. Transient wave propagation in piezoelectric half space. Zeitschrift Fur Angewandte Mathematik Und Physik (ZAMP) 51, 236–266.

Li, S., 2001. On diffraction in a piezoelectric medium by a half-plane: the Sommerfeld problem. Zeitschrift Fur Angewandte Mathematik Und Physik (ZAMP) 52, 101–134.

Li, S., To, A.C., Glaser, S.D., 2005. On scattering in a piezoelectric medium by a conducting crack. J. Appl. Mech. 72, 943–954.

Li, X.-F., Tang, G.J., 2003. Transient response of a piezoelectric ceramic strip with an eccentric crack under electromechanical impacts. Int. J. Solids Struct. 40, 3571–3588.

Ma, L., Wu, L.-Z., Zhou, Z.-G., Guo, L.-C., 2005. Scattering of the harmonic anti-plane shear waves by a crack in functionally graded piezoelectric materials. Composite Struct. 69, 436–441.

Meguid, S.A., Chen, Z.T., 2001. Transient response of a finite piezoelectric strip containing coplanar insulating cracks under electromechanical impact. Mech. Mater. 33, 85–96.

Melkumyan, A., 2005a. Comments on ''Dynamic crack propagation in piezoelectric materials—Part I. Electrode solution'' by Shaofan Li, Peter A. Mataga [J. Mech. Phys. Solids 44 (1996) 1799–1830]. J. Mech. Phys. Solids 53, 1918–1925.

Melkumyan, A., 2005b. Comments on ''Explicit transient solutions for a mode III crack subjected to dynamic concentrated loading in a piezoelectric material'' by Yi-Shyong Ing, Mau-Jung Wang [Int. J. Solids Struct. 41 (2004) 3849–3864]. Int. J. Solids Struct. 42, 6700–6704.

Melkumyan, A., 2005c. Diffraction of nonstationary waves generated by a force applied on a face of a crack in piezoelectric medium in the cases of presence and absence of an electrode. Proc. Natl. Acad. Sci. Armenia, Mech. 58 (2), 28–41.

Melkumyan, A., 2005d. Dynamic propagation of a semi-infinite crack with constant velocity in piezoelectric medium. Proc. Natl. Acad. Sci. Armenia, Mech. 58 (4), 59–74.

Melkumyan, A., 2006. On acoustic and electric waves diffraction in piezoelectric medium by a permeable half-plane crack. Zeitschrift Fur Angewandte Mathematik Und Physik (ZAMP), doi:10.1007/s00033-006-0076-3.

Narita, F., Shindo, Y., 1998. Dynamic anti-plane shear of a cracked piezoelectric ceramic. Theor. Appl. Fracture Mech. 29, 169–180.

Noble, B., 1958. Methods based on the Wiener–Hopf technique. Pergamon Press, New-York.

Parton, V.Z., Kudryavtsev, B.A., 1988. Electromagnetoelasticity. Gordon and Beach, New York.

Shindo, Y., Narita, F., Ozawa, E., 1999. Impact response of a finite crack in an orthotropic piezoelectric ceramic. Acta Mechanica 137, 99–107.

To, A.C., Li, S., Glaser, S.D., 2005. On scattering in dissimilar piezoelectric materials by a semi-infinite interfacial crack. Q. J. Mech. Appl. Math. 58 (2), 309–331.

To, A.C., Li, S., Glaser, S.D., 2006. Interfacial crack propagation in dissimilar piezoelectric materials. Wave Motion 43, 368–386.

Ueda, S., 2003a. Transient response of sandwiched piezoelectric strip with crack normal to interface under impact. Theor. Appl. Fracture Mech. 40, 211–223.

Ueda, S., 2003b. Transient dynamic response of a coated piezoelectric strip with a vertical crack. Eur. J. Mech. A/Solids 22, 925–942.